

CONSTITUTIVE MODEL FOR CONCRETE UNDER NON-PROPORTIONAL LOADING

E. Mizuno
Department of Civil Engineering, Nagoya University,
Japan

S. Hatanaka
Department of Architecture, Mie University,
Japan

Abstract

The first objective in the present paper is to propose a constitutive model to represent the softening behavior of concrete under a general stress state. The second objective is to show the efficiency of the model by comparing the model prediction with experimental data under non-proportional loading paths.

In the first half of the present paper, the authors' constitutive softening model is developed in detail to predict softening behavior under a general stress state. In the second half of the paper, the outline of the experiment for non-proportional loading is explained, and model predictions are compared with the triaxial compression test data under non-proportional loading.

Key words: Constitutive model, softening, non-proportional loading, and plasticity

1 Introduction

The softening behavior of concrete materials affects greatly the plastic deformation of reinforced concrete (RC) structures or members. Therefore, in order to evaluate the plastic-deformation capacity of RC

structures or members from the finite element analysis, it becomes very important to develop and apply a sophisticated concrete model. The concrete model has recently been required to represent the moderate softening behavior under a multi-dimensional stress state, which changes non-proportionally in the finite element analysis.

So far, there has been research developing a concrete softening model under multi-dimensional stress conditions (Bazant and Bhat, 1976; Bazant and Kim, 1979; Ortiz, 1985; Han and Chen, 1986; Kioussis, 1987; Ohtani and Chen, 1989; Wu and Tanabe, 1990; Hasegawa and Bazant, 1993; Pallewatta, et. al, 1995). Among these, some of the concrete models have been examined for their representation capacity to predict the softening behavior under reversed loading conditions (unloading/reloading conditions). As far as the authors know, however, it is difficult to find research that has evaluated the capability of the constitutive model to represent concrete behavior under non-proportional loading path, because reliable experimental work to analyze such a loading path has rarely been performed.

In order to provide the experimental data for use in the calibration of a concrete model, one of the authors has performed a triaxial compression test on a cubic concrete specimen ($10 \times 10 \times 10$ cm) under a relatively low confining pressure, i.e., approximately 1.96 MPa (20 kgf/cm^2) (Kosaka, et. al, 1984; Hatanaka, et. al, 1987). The loading applied in the triaxial compression test are classified as one of two types. The first is a proportional loading under constant lateral confining pressure. The other is a non-proportional loading under (1) gradually increasing lateral confining pressure, (2) suddenly increasing lateral confining pressure, and (3) suddenly decreasing lateral confining pressure. Utilizing the experimental data under constant lateral confining pressure, the authors have developed a strain-space based-plasticity model (Mizuno and Hatanaka, 1992) to theoretically investigate the compressive softening behavior of concrete under a proportional loading and then confirmed its representation capacity with a triaxial compression test.

The first objective in the present paper is to propose a constitutive model to represent the softening behavior of concrete under a general stress state. The second objective is to show the efficiency of the model by comparing the model prediction with the author's experimental data under non-proportional loading paths.

In the first half of the present paper, the authors' constitutive softening model is developed in detail to predict softening behavior under a general stress state. In the second half of the paper, the outline of the experiment for non-proportional loading is explained, and model predictions are compared with the triaxial compression test data under non-proportional loading.

2 Softening model

2.1 Outlines of softening model

A compressive softening model for concrete (Mizuno and Hatanaka, 1992) has been extended to a model with which the tensile behavior of concrete can also be handled. In this Section, the outlines of the proposed model will be presented and the model parameters will be re-examined.

2.1.1 Functions F and G

The proposed softening model is based on the plasticity theory defined in strain space. Therefore, the stress-strain incremental is formulated under the assumption of the non-associated flow rule, using the loading function F and the plastic potential function G defined in strain space. The function F and G are generally written as follows:

$$F = F \left[\bar{I}_1, \sqrt{\bar{J}_2}, \theta, m, F_p, f_c', a \right] = 0 \quad (1)$$

$$G = G \left[\bar{I}_1, \sqrt{\bar{J}_2}, \theta, m, k, F_p, f_c', a \right] = 0 \quad (2)$$

where \bar{I}_1 is the first invariant of elastic strain tensor; \bar{J}_2 is the second invariant of elastic deviatoric strain tensor; θ is the Lode angle; m is the parameter related to the curvature of meridian of the failure surface; F_p is the strength parameter representing the size of the failure surface; k is the parameter to relate the failure surface and the plastic potential surface ($F = G$ in the case of $k = 1$); f_c' is the uniaxial compressive strength of concrete; and a is the parameter related to the tensile strength of concrete.

Both functions F and G can be schematically viewed in strain invariant space (\bar{I}_1, \bar{J}_2) , as shown in Fig.1. More details for these functions are presented as Eq.(a) and Eq.(c) in Table 1. As can be understood from these equations, all the variables in the equations are normalized by the uniaxial compressive strength of concrete, f_c' .

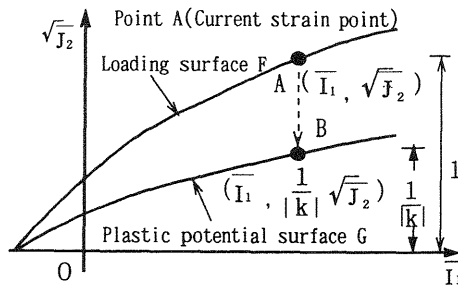


Fig.1 Loading surface and plastic Potential surface

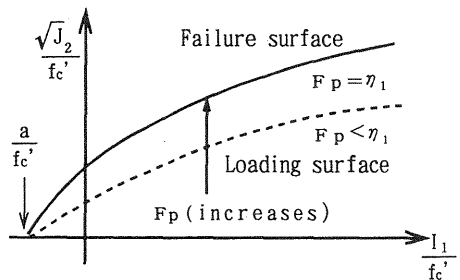


Fig.2 Loading surface in stress space

2.1.2 Determination of model parameters a , m , and η_I

The loading surface expands isotropically as the strength parameter F_p increases with the increment of plastic work. With further increases in plastic work, the loading surface becomes a failure surface of maximum size when F_p takes its maximum value (i.e., η_I), as shown in Fig.2. After this, the loading surface gradually shrinks in its size with a decrease in the F_p value. The substitution of $F_p = \eta_I$ into Eq.(2) leads to the failure surface defined in the strain space, which is equivalent to the failure surface (Eq.(b) in Table 1) defined in the non-dimensional stress invariant space.

The parameters a , m , and η_I involved in the failure surface (the Lade type of failure surface is used in the present study) can be calibrated by using the triaxial compression test data under several confining pressures.

In order to calibrate parameter a , we consider three types of tensile failures under principal stress conditions, as shown in Fig.3. In the present modeling of tensile failure, the triaxial tensile failure state $(\sigma_1, \sigma_2, \sigma_3) = (f_t, f_t, f_t)$ shown in Fig.3(c) is assumed to be equivalent to the apex of the failure surface on the hydrostatic pressure axis, I_1 . Here, f_t is the tensile strength of concrete and is assumed to be one-tenth the compressive strength, f_c . Therefore, the apex of the failure surface passes through the point $(I_1/f_c, \sqrt{J_2}/f_c) = (-0.3, 0)$ in stress invariant space. In this case, parameter a takes the value of $0.3 f_c$.

The other parameters m and η_I can be determined under the following conditions:

- 1) The compressive meridian of the failure surface at the Lode angle $\theta = 60^\circ$ passes through a point $(I_1/f_c, \sqrt{J_2}/f_c) = (1.0, 1/\sqrt{3})$ which is the uniaxial compression failure point.
- 2) The failure surface is fit particularly within $I_1/f_c = 10$ by the least squares method, with failure points from several triaxial compression tests and biaxial compression/tension tests (see Figs.4 and 5).

As a result, $m = 1.0$ and $\eta_I = 224.5$ are evaluated, respectively.

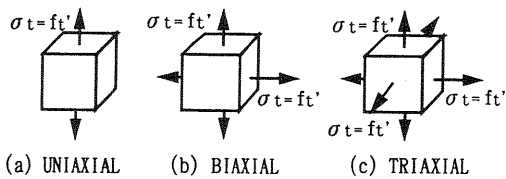


Fig.3 Failure type in tension

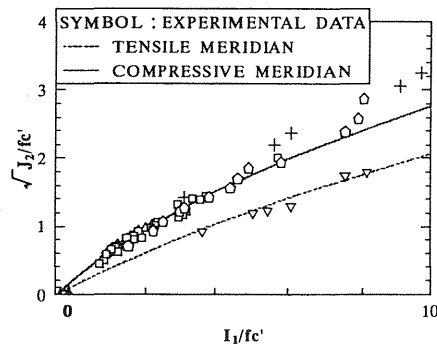


Fig.4 Failure surface and Experimental data

2.2 Strength parameter F_p – non-dimensional plastic work W_p/P_a

The strength parameter F_p increases in the hardening state, reaching its maximum value at the failure state and then decreasing in the softening state. It can be expressed in terms of the non-dimensional plastic work W_p/P_a where P_a is the atmospheric pressure, as can be shown in Fig.6. The plastic work W_p is given by

$$W_p = \int \sigma_{ij} d\varepsilon_{ij}^p \quad (3)$$

where σ_{ij} is the stress tensor and $d\varepsilon_{ij}^p$ is the incremental plastic strain tensor.

2.2.1 $F_p - W_p/P_a$ relation under constant confining pressure

It has been observed from the triaxial compression test that the $F_p - W_p/P_a$ relation tends to become ductile as the confining pressure increases, as shown schematically in Fig.6 (Mizuno and Hatanaka, 1992). This relation involves the following two parameters: the first is parameter γ that affects the slope of the stress-strain curve in the softening range, and the other is parameter W_{ppeak}/P_a that is the non-dimensional plastic work accumulated up to the failure state.

These two parameters were originally assumed to be a function of confining pressure σ_c only (Mizuno and Hatanaka, 1992). In the present study, however, by introducing the non-dimensional variable σ_c/f_c' , the strength parameter F_p can be given by

$$F_p = F_p \left[W_p / P_a, \gamma(\sigma_c / f_c'), W_{ppeak} / P_a(\sigma_c / f_c') \right] \quad (4)$$

Noted that γ and W_{ppeak} have constant values under constant confining pressure. The detailed expression for F_p is shown as Eq.(d) in Table 1.

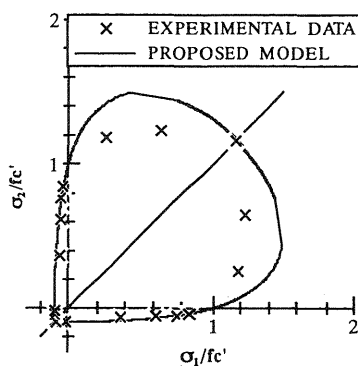


Fig.5 Failure surface in biaxial stress space

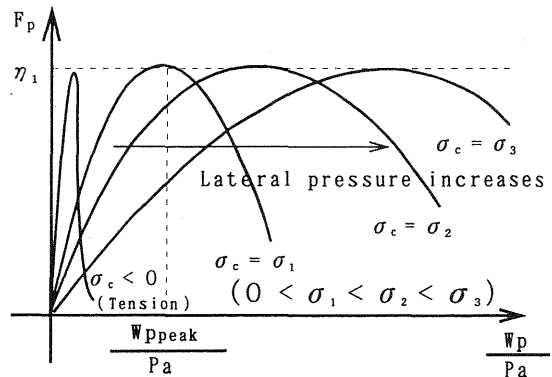


Fig.6 $F_p - W_p$ relation

2.2.2 $F_p - W_p/P_a$ relation under varying confining pressure

The stress path in the triaxial compression test under constant confining pressure becomes a straight line with a slope of $1/\sqrt{3}$ in non-dimensional stress invariant space, for example, path (O-O') or path (C-C'), as shown in Fig.7. Therefore, it becomes possible to observe the $F_p - W_p/P_a$ relation from the triaxial compression test data. In other words, once the $F_p - W_p/P_a$ relation under an arbitrary constant confining pressure is formulated, the stress-strain curve under an arbitrary constant confining pressure can be predicted analytically.

In the finite element analysis on RC structures, on the other hand, the stress path inside concrete takes generally a random path, i.e., Path A-B'-C' at the Lode angle $\theta = 60^\circ$, as shown Fig.7. Therefore, it may not be clear what kind of $F_p - W_p/P_a$ relation under constant confining pressure should be used in the analysis to determine the stiffness dF_p/dW_p at an arbitrary point on the random path.

In the present study, in order to determine the $F_p - W_p/P_a$ curve for a random path, we introduce the concept of equivalent confining pressure in the following. The equivalent confining pressure to the stress point B' on a random stress path (A-B'-C') is assumed to be hydrostatic pressure ($\sigma_b, \sigma_b, \sigma_b$) at point B in Fig.7. Point B is the intersection point on the hydrostatic pressure axis with a straight line having a slope of $1/\sqrt{3}$.

Therefore, the $F_p - W_p/P_a$ curve can be obtained by substituting $\sigma_c = \sigma_b$ into Eq.(4), and the stiffness dF_p/dW_p at an arbitrary point B' on the random path can thus be evaluated for use in the finite element analysis.

2.3 Model parameters

2.3.1 Parameters γ and W_{ppeak} under compressive equivalent-confining pressure

A set of parameters γ and W_{ppeak} under compressive equivalent-confining pressure can be obtained from the least squares method by using the triaxial compression test data under constant compressive confining pressure σ_c . From these data, the $\gamma - \sigma_c/f_c'$ relation and $W_{ppeak} - \sigma_c/f_c'$ relation in

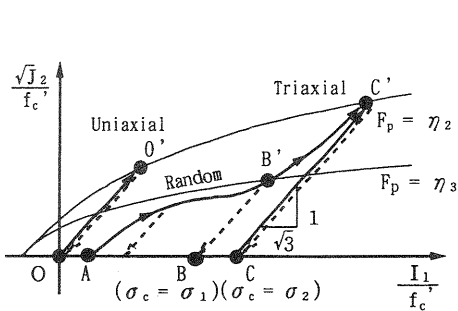


Fig.7 Stress paths in experiment

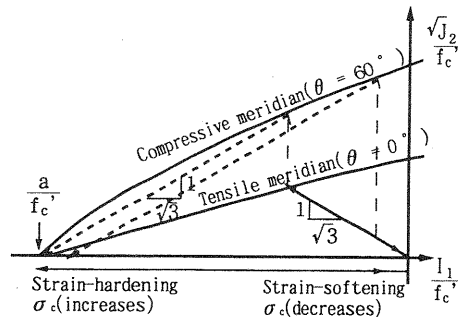


Fig.8 Equivalent confining pressure in tension test

compressive equivalent-confining pressure are given in Eqs.(e) and (g) in Table 1.

2.3.2 Parameters γ and W_{ppeak} under tensile equivalent-confining pressure

The γ - σ_c/f_c' relation and W_{ppeak}/P_a - σ_c/f_c' relation under tensile equivalent-confining pressure cannot be generally obtained due to the lack of triaxial compression test data under constant tensile confining pressure σ_c . In the present modeling, therefore, using the existing tensile test data on a concrete specimen with several different compression strengths, these relations are calibrated under the following conditions:

- 1) In order for the model to predict the uniaxial tensile behavior under the stress path shown in Fig.8, the W_{ppeak}/P_a value is assumed to reduce linearly in a range of $-0.01 < \sigma_c/f_c' < 0$, with an increase in the equivalent tensile confining pressure, as shown in Fig.9.
- 2) According to experimental data, the bigger the uniaxial tensile strength, the more the concrete specimen absorbs plastic energy up to the tensile failure stage. The W_{ppeak}/P_a value ($F_{0.01}$) at $\sigma_c/f_c' = -0.01$ is assumed to be a function of the uniaxial compression strength f_c' .
- 3) For the range $\sigma_c/f_c' < -0.01$, the W_{ppeak}/P_a is assumed to show a similar reduction.
- 4) As for parameter γ , it is assumed to take a constant value γ_0 in a tensile range of $\sigma_c/f_c' < 0$.

These relations are expressed as Eqs.(f), (h), \sim (l) in Table 1.

2.3.3 Parameter k

Since the plastic volumetric strain (dilatancy) reduces as the values of parameter k become larger, the axial stress - lateral strain curve of concrete specimen tends to be steep in softening range.

In the hardening range, parameter k is assumed to be a function of the strength parameter F_p , as shown in Eqs.(m), (n), and (o) in Table 1.

On the other hand, it is known from the authors' work that the value for parameter k in the softening range becomes larger as the strength

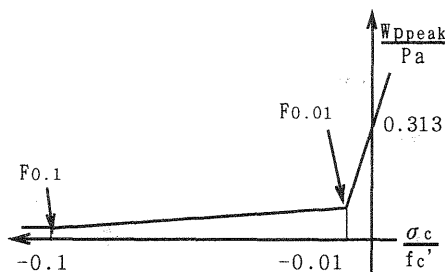


Fig.9 W_{ppeak}/P_a reduction in tension

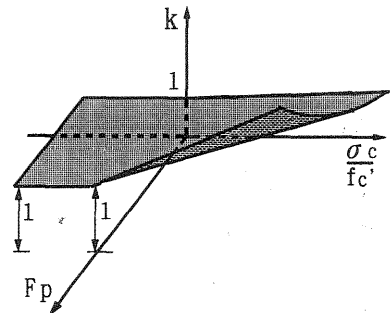


Fig.10 k variation in softening

Table 1 Parameters for the concrete softening model

Loading Function	Strain space	(a)
	$F = \left(-\frac{3K}{f_c'} \bar{I}_1 + \frac{a}{f_c'} \right)^3 - \left[27 + F_p \left(-\frac{3K}{f_c'} \bar{I}_1 + \frac{a}{f_c'} \right)^{-m} \right] \times \left[\frac{1}{27} \left(-\frac{3K}{f_c'} \bar{I}_1 + \frac{a}{f_c'} \right)^3 - \frac{1}{3} \left(-\frac{3K}{f_c'} \bar{I}_1 + \frac{a}{f_c'} \right) \left(\frac{2G}{f_c'} \sqrt{J_2} \right)^2 - \frac{2}{3\sqrt{3}} \cos 3\theta \left(\frac{2G}{f_c'} \sqrt{J_2} \right)^3 \right] = 0$	
	Stress space	(b)
	$f = \left(-\frac{I_1}{f_c'} + \frac{a}{f_c'} \right)^3 - \left[27 + F_p \left(-\frac{I_1}{f_c'} + \frac{a}{f_c'} \right)^{-m} \right] \times \left[\frac{1}{27} \left(-\frac{I_1}{f_c'} + \frac{a}{f_c'} \right)^3 - \frac{1}{3} \left(-\frac{I_1}{f_c'} + \frac{a}{f_c'} \right) \left(\frac{\sqrt{J_2}}{f_c'} \right)^2 - \frac{2}{3\sqrt{3}} \cos 3\theta \left(\frac{\sqrt{J_2}}{f_c'} \right)^3 \right] = 0$	
Plastic potential function	$G = \left(-\frac{3K}{f_c'} \bar{I}_1 + \frac{a}{f_c'} \right)^3 - \left[27 + F_p \left(-\frac{3K}{f_c'} \bar{I}_1 + \frac{a}{f_c'} \right)^{-m} \right] \times \left[\frac{1}{27} \left(-\frac{3K}{f_c'} \bar{I}_1 + \frac{a}{f_c'} \right)^3 - \frac{1}{3} \left(-\frac{3K}{f_c'} \bar{I}_1 + \frac{a}{f_c'} \right) \left(\frac{2G}{f_c'} \frac{\sqrt{J_2}}{ k } \right)^2 - \frac{2}{3\sqrt{3}} \cos 3\theta \left(\frac{2G}{f_c'} \frac{\sqrt{J_2}}{ k } \right)^3 \right] = 0$	(c)
$F_p - Wp/P_a$	$F_p = \alpha \left(\frac{Wp}{Pa} \right)^{\frac{1}{\gamma}} \exp \left(-\beta \frac{Wp}{Pa} \right) \quad \text{where } \alpha = \eta_1 \left(\frac{ePa}{Wp_{peak}} \right)^{\frac{1}{\gamma}} \quad \beta = \frac{Pa}{\gamma Wp_{peak}}$	(d)
$\gamma - \sigma_c / f_c'$	$\gamma = 2.97 \left(\frac{\sigma_c}{f_c'} \right)^{0.243} + \gamma_0 \quad (\text{Compression } \sigma_c / f_c' \geq 0)$	(e)
	$\gamma = \gamma^0 = 1.95 \quad (\text{Tension } \sigma_c / f_c' < 0)$	(f)
$Wp_{peak}/Pa - \sigma_c / f_c'$	$\frac{Wp_{peak}}{Pa} = 29.8 \left(\frac{\sigma_c}{f_c'} \right)^{0.995} + \frac{Wp_{peak}^0}{Pa} \quad (\sigma_c / f_c' \geq 0)$	(g)
	$\frac{Wp_{peak}}{Pa} = 100 \times \left(\frac{Wp_{peak}^0}{Pa} - F_{0.01} \right) \times \frac{\sigma_c}{f_c'} + \frac{Wp_{peak}^0}{Pa} \quad (-0.01 \leq \sigma_c / f_c' < 0)$	(h)
	$\frac{Wp_{peak}}{Pa} = \frac{(F_{0.1} - F_{0.01})}{(-0.1 + 0.01)} \times \left(\frac{\sigma_c}{f_c'} + 0.01 \right) + F_{0.01} \quad (-0.1 \leq \sigma_c / f_c' < -0.01)$	(i)
	$\frac{Wp_{peak}}{Pa} = F_{0.1} \quad (\sigma_c / f_c' < -0.1)$	(j)
	$\text{where } F_{0.01} = 5.14 \times 10^{-9} (f_c')^2 + 3.91 \times 10^{-5} \quad (\sigma_c / f_c' = -0.01)$ $F_{0.1} = 1.97 \times 10^{-9} (f_c')^2 + 1.07 \times 10^{-5} \quad (\sigma_c / f_c' = -0.1)$	(k) (l)
Parameter k	Strain - hardening	(m)
	Elastic	$(0 \leq F_p < 50)$
	$k = F_p - 70$	$(50 \leq F_p < 60)$
	$k = -10$	$(60 \leq F_p < 224.5)$
	Strain - softening	(p)
$k = b \left(\frac{\sigma_c}{f_c'} \right) + c$	$(\sigma_c / f_c' \geq 0)$	
$k = 1$	$(\sigma_c / f_c' < 0)$	
where	$b = 2.27 \times 10^{-3} (F_p + 8.6 \times 10^{-3})^{1.9} - 3.26 \times 10^{-7}$ $c = 3.1 \times 10^{-4} (F_p) + 9.4 \times 10^{-1}$	(q)

$a = 0.3f_c'$ $m = 1.0$ $\eta_1 = 224.5$ I_1, J_2 : Stress invariants \bar{I}_1, \bar{J}_2 : Elastic strain invariants θ : Lode angle K : Bulk elastic modulus
 G : Shear elastic modulus F_p : Strength Parameter k : Parameter related to function G e : Logarithmic base
 P_a : Atmospheric pressure σ_c : Equivalent confining pressure f_c' : Uniaxial compressive strength $\gamma^0 = 1.95$ $Wp_{peak}^0 / Pa = 0.313$

parameter F_p and the confining pressure σ_c become large, as shown in Fig.10. In the case where the equivalent confining pressure σ_c is in the compression range, the k value is given by

$$k = b \times (\sigma_c / f_c') + c \quad (5)$$

where coefficients b and c can be referred to in Table 1. The k value is found to be more than 1.0, which means that the non-associated flow rule can be applied. On the other hand, in the case where the equivalent confining pressure is in the tensile range, k is assumed to be 1.0 (the associated flow rule is applied).

3 Experiment and model verification

3.1 Experiment type

Variation of the lateral confining pressure in the experiment under non-proportional loading is shown in Tables 2 through 4. The specimens used in the experiment were with the size of $10 \times 10 \times 10$ cm cubes and were prepared for three different water/cement ratios (W/C) = 0.45, 0.55, and 0.70. The uniaxial compressive strengths f_c' for concrete specimens with these water/cement ratios were 32.3, 25.7, and 20.2 MPa, respectively.

The confining pressures applied in the test can be classified as three different types: (1) a gradually increasing confining pressure (Type I), (2) a suddenly increasing confining pressure (Type II), and (3) a suddenly decreasing confining pressure (Type III). In Type I, the lateral pressure is passively applied to the specimen with increasing axial strain under a hydrostatic pressure state (see Fig.11(a)). In Type II (III), the lateral pressure is applied (removed) at a certain strain level beyond the strain at the peak stress. The schematic loading for Type III is shown in Fig.12(a).

3.2 Model verification

Figures 11 and 12 show the loading scheme, the loading path in stress invariant space, and a model comparison with experimental data. In the following, the model capability is verified with two types of test results

Table 2 Variation of σ_c
In experiment Type I

W/C	Case 1 ($\times 10^{-1}$ MPa)	Case 2 ($\times 10^{-1}$ MPa)	Case 3 ($\times 10^{-1}$ MPa)
0.45	0.23→6.93	0.57→13.1	7.35→9.8
0.55	0.0 →6.25	0.57→11.1	6.96→9.8
0.70	0.45→3.98	0.45→6.25	3.69→4.37

Table 3 Variation of σ_c
In experiment Type II

W/C=0.55	Strain at loading (%)	Stress at loading (MPa)
Case 1	0.30	0.76
Case 2	0.55	0.79
Case 3	1.00	0.83

Table 4 Variation of σ_c in experiment Type III

W/C=0.55	Initial confining pressure (MPa)	Strain at unloading (%)	Lateral stress at unloading (MPa)	W/C=0.70	Initial confining pressure (MPa)	Strain at unloading (%)	Lateral stress at unloading (MPa)
Case 1	0.735	0.30	0.764	Case 1	0.735	0.35	0.76
Case 2	0.735	0.60	0.794	Case 2	0.735	1.00	0.83
Case 3	0.735	1.05	0.843	Case 3	0.735	1.60	0.89
Case 4	0.735	1.50	0.882				

under non-proportional loading, among all the experimental results.

3.2.1 Predictions under gradually increasing lateral confining pressures
 As a numerical example, a comparison of the model predictions is made with the test data for a concrete specimen with W/C (water/cement ratio) = 0.55, as shown in Fig.11(c). The bulk and shear moduli used in the analysis are 14,700 MPa and 11,025 MPa, respectively. It can be found from the test that the variation in confining pressure affects the residual compressive strength. In particular, the residual compressive strength at 2 % axial strain under Case 3 is larger than that under Case 2, where the confining pressure leads up to 1.11 MPa at 2 % axial strain level (larger than 0.98 MPa in Case 3). It can be seen from the figure that the proposed model can represent a path-dependent behavior under gradually increasing lateral confining pressure reasonably well.

3.2.2 Predictions under suddenly decreasing lateral confining pressures
 As a numerical example, in Fig.12(c), the model prediction is compared with the test data for the concrete specimen with W/C (water/cement ratio) = 0.55. While the confining pressure decreases, the stress state inside the specimen becomes a loading state (Path II). As the axial compression load is applied again, the specimen behaves elasto-plastically, followed by softening (Path III). The present model can represent a path-dependent behavior for which the axial compression strength immediately after the reduction of the confining pressure is larger than that after the uniaxial compression test.

4 Conclusions and summary

The following conclusions and summary can be made from this study:

- 1) The compressive softening concrete model was extended to a model, which can also treat tensile softening behavior without violating any of the assumptions made in the previous study.
- 2) The Lade type of three parameter loading surface was adopted in this study; however, any kind of function can be applied as a loading function in the proposed model.
- 3) The capabilities of the model, which represents the non-proportional

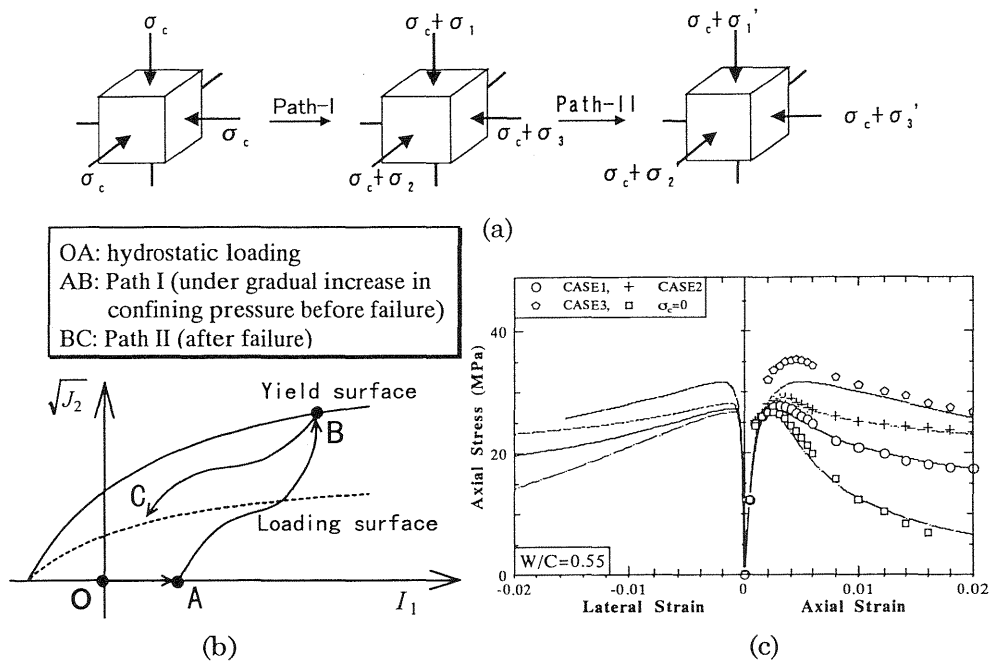


Fig.11 Concrete behavior under gradually increasing lateral pressure

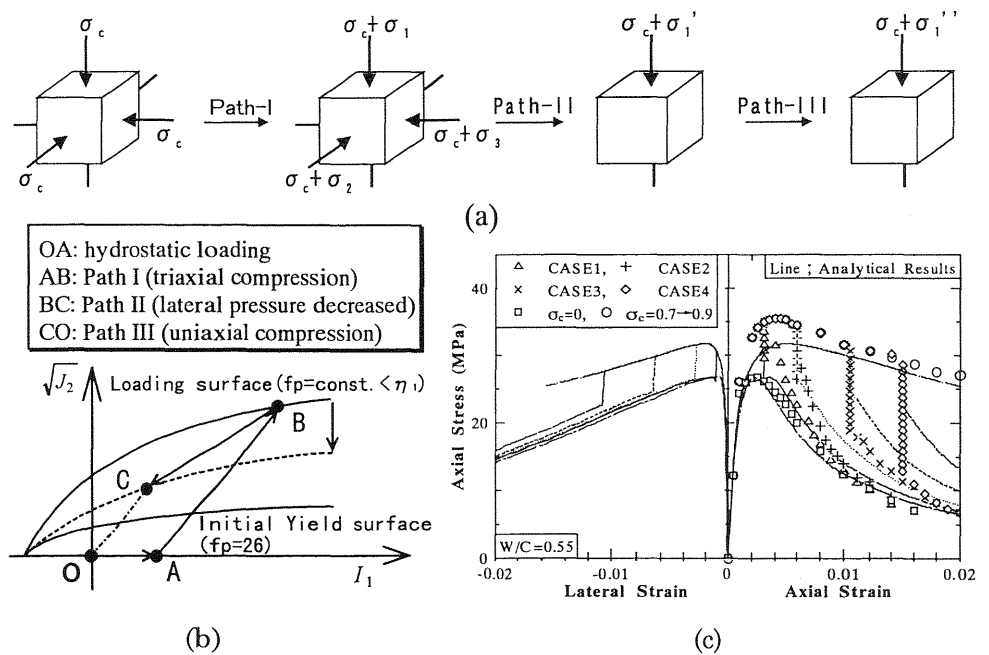


Fig.12 Concrete behavior under suddenly decreasing lateral pressure

behavior of concrete under a general stress state, were examined using two types of non-proportional loading paths under i) gradually increasing confining pressure and ii) suddenly decreasing confining pressure.

- 4) As a result of a comparison with test data, it was found that the proposed model accurately represents the non-proportional behavior.
- 5) The model should be applied to structural analyses to evaluate its applicability.

5 References

- Bazant, Z.P. and Bhat, P.D. (1976) Endochronic theory of inelasticity and failure of concrete. **J. Engrg. Mechanics, ASCE**, 102(4), 701-722.
- Bazant, Z.P. and Kim, S.S. (1979) Plastic-fracturing theory for concrete. **J. Engineering Mechanics, ASCE**, 105(3), 407-428.
- Han, D.J. and Chen, W.F. (1986) Strain-space plasticity formulation for hardening-softening materials with elasto-plastic coupling. **Int. J. Solids Structures**, 22(8), 935-950.
- Hasegawa, T. and Bazant, Z.P. (1993). Nonlocal microplane concrete model with rate effect and load cycles, **J. Materials in Civil Engrg., ASCE**, 5(3), 372-410.
- Hatanaka, S., Kosaka, Y. and Tanigawa, Y. (1987) Plastic deformational behavior of axially loaded concrete under low lateral pressure – An evaluation method for compressive toughness of laterally confined concretes (Part I). **J. Struct. Construct. Engrg.**, Tokyo, 377, 27-40.
- Kiousis, P.D. (1987) Strain space approach for softening plasticity. **J. Engineering Mechanics, ASCE**, 102(4), 701-722.
- Kosaka, Y., Tanigawa, Y., and Hatanaka, S. (1984) Inelastic deformational behavior of axially loaded concrete under low lateral stresses. **Trans. Japan Concrete Institute**, 6, 257-260.
- Mizuno, E. and Hatanaka, S. (1992) Compressive softening model for concrete. **J. Engineering Mechanics, ASCE**, 118(2), 1546-1563.
- Ohtani, Y. and Chen, W.F. (1989) A plastic-softening model for concrete materials. **Computers & Structures**, 33(4), 1047-1055.
- Ortiz, M. (1985) A constitutive theory for the inelastic behavior of concrete, **Mechanics of Materials** 4, 67-93.
- Pallewatta, T.M., Irawan, P. and Maekawa, K. (1995) Verification of 3D constitutive model of concrete in line with capacity and ductility of laterally reinforced concrete columns. **J. Materials, Conc. Struct., Pavements**, 520/28, 309-321.
- Wu, Z. and Tanabe, T. (1990) A hardening/softening model of concrete subjected to compressive loading. **J. Struct. Engrg., JSCE**, 36B, 153-162.